A Stable Spectral Difference Method for Triangles

Aravind Balan[*] and Georg May[†]

Graduate School AICES, RWTH Aachen University, Aachen, Germany

Joachim Schöberl[‡]

Institute for Analysis and Scientific Computing, Vienna Technical University, Vienna, Austria

Numerical schemes using piecewise continuous polynomials are very popular for high order approximation of conservation laws. While the most widely used numerical scheme under this paradigm appears to be the Discontinuous Galerkin method, the Spectral Difference scheme has often been found attractive as well, because of its simplicity of formulation and implementation. However, recently it has been shown that the scheme is not unconditionally linearly stable on triangles. In this paper we present an alternate formulation of the scheme, featuring a new flux interpolation technique using Raviart-Thomas spaces, which proves stable under a similar linear analysis in which the standard scheme failed. We demonstrate viability of the concept by showing linear stability both in the semi-discrete sense and for time stepping schemes of the SSP Runge-Kutta type. Furthermore, we present a convergence study using the linear advection equation, as well as case studies in compressible flow simulation using the Euler equations.

I. Introduction

For some time now a considerable amount of research activity has been devoted to high-order methods for the simulation of compressible fluid flow. In particular schemes based on piecewise continuous polynomial approximation, such as Discontinuous Galerkin (DG) methods[5–9] became increasingly popular.

Even for moderate levels of accuracy, high-order methods are potentially more efficient than low-order methods in terms of total degrees of freedom. However, for such problems, low order methods are still widely used as they have proved to be reliable and stable. For high-order methods to be viable in this context, they should be stable, robust and easy to implement. It is in this context that the SD scheme has been proposed as a collocation method derived from the strong form of the governing equations.[1–3] Recently, the connection between the Spectral Difference (SD) scheme and the weak form of the governing equations has been highlighted by several authors, and the scheme has been put into a more general framework using unifying formulations such as Huynh's flux reconstruction schemes,[?] or Wang's lifting collocation penalty schemes.[?] By using the 'quadrature-free' paradigm,[?] equivalence with nodal Discontinuous Galerkin methods can be established in particular for nonlinear conservation laws.[4] The Spectral Difference scheme seems to be particularly attractive as there are no surface or volume integrals to be computed.

The SD scheme has been found to be stable for one dimensional linear advection problems by Jameson[10] for all orders of accuracy in an energy norm of Sobolev type. Accuracy and stability are found to be independent of the position of the solution points in most cases, which makes the design simpler.[11] But linear stability analysis performed by Van den Abeele et al.[11] shows that the scheme in its standard formulation is unstable for order of accuracy greater than two on triangular meshes. The new variant of the Spectral Difference scheme, which was proposed by May and Schöberl,[12] is formulated by incorporating a new interpolation technique into the standard Spectral Difference scheme. In this scheme, the flux function of the conservation law is approximated by projecting it onto the Raviart-Thomas (RT) space. For triangular meshes, the scheme proved stable under linear stability analysis for periodic problems for which the standard

---

Spectral Difference scheme was found unstable.[12] Further, the RT space demands fewer degrees of freedom for the same order of accuracy than the standard scheme, which means a reduction in computational cost.

In the present paper we build on the stability analysis in,[12] and construct stable RT-based nodal elements for flux interpolation having divergence in the space of linear, quadratic, and cubic polynomials. We consider linear stability analysis of the RT-based SD scheme for the semi-discrete case as well as the fully discrete case using time stepping schemes of the SSP Runge-Kutta type.[15] Furthermore we demonstrate viability of the new SD scheme with case studies using the scalar advection equation and the Euler equations.

II.   The Spectral Difference Scheme for Triangles

We present here the derivation of the SD scheme from the strong form of the governing equations as given in the original formulation of the scheme.[1] Consider the scalar hyperbolic conservation equation

$$\frac{\partial u(x,t)}{\partial t} + \nabla^x \cdot \vec{f}(u) = 0 \tag{1}$$

on some domain $(x,t) \in \Omega \times \mathbb{R}^+$, where $\Omega \subset \mathbb{R}^2$ in the present case. Note that we reserve vector notation for the flux function, as this will prove useful for highlighting the differences in the flux interpolation between the standard SD scheme, derived in this section, and the new scheme. Consider a triangulation of the domain, $T_h = \{T^{(i)}, i = 1, ..., N_T\}$ which decomposes the domain Ω into N_T cells, where each cell is denoted by the index i as a bracketed superscript. However, the formulations given below hold for each cell and the superscript is omitted to avoid confusion and is shown only in the final form of the equation. For convenience, the SD scheme is formulated for a reference triangle. We consider the transformation from the reference domain (ξ) to the physical domain (x) for each triangular cell which is defined by the invertible mapping $\Phi : \xi \mapsto x$ with a non-singular Jacobian, $J = \partial x/\partial \xi$, such that each element in the triangulation can be mapped to a reference domain $\hat{T} = \Phi^{-1}(T)$. Two sets of points are defined in the reference domain. The first set, $\hat{\xi}_j$, $j = 1, ..., N_m$, is for the solution collocation and the second one, $\breve{\xi}_k$, $k = 1, ..., N_{m+1}$, is for the flux collocation. In the reference domain, the above hyperbolic equation is of the form

$$\frac{\partial u(\xi,t)}{\partial t} + \frac{1}{|J|}\nabla^\xi \cdot \left(|J|J^{-1}\vec{f}(u)\right) = 0. \tag{2}$$

Now the solution function u in the reference domain is approximated to u_h by projecting it onto a finite dimensional polynomial space as

$$u_h(\xi) = \sum_{j=1}^{N_m} u_j l_j(\xi), \tag{3}$$

where $l_j(\xi)$, $j = 1, .., N_m$ are the Lagrangian interpolation functions, defined by the solution collocation nodes with the property $l_k(\hat{\xi}_j) = \delta_{jk}$ and hence the coefficients are given as $u_j = u_h\left(\hat{\xi}_j\right)$. These Lagrangian functions form a basis in the finite dimensional polynomial space of degree m, denoted as P_m. In 2D, the number of degrees of freedom required to represent a function in the space P_m is given as

$$N_m = \frac{(m+1)(m+2)}{2}. \tag{4}$$

The flux function in the reference domain, which is defined as $|J|J^{-1}\vec{f}$, is approximated by $\vec{f}_h$, by projecting it component-wise into a finite dimensional polynomial space of degree $m + 1$ as

$$\vec{f}_h(\xi) = \sum_{k=1}^{N_{m+1}} \vec{f}_k \hat{l}_k(\xi), \tag{5}$$

where $\hat{l}_k(\xi)$, $k = 1, .., N_{m+1}$ are the Lagrangian interpolation functions, defined by the flux collocation nodes with the property $\hat{l}_k(\breve{\xi}_j) = \delta_{jk}$. The coefficients of the interpolation are defined as

$$\vec{f}_k = \begin{cases} |J|J^{-1}\vec{f}\left(\breve{\xi}_k\right), & \breve{\xi}_k \in \hat{T}, \\ \vec{f}_{num} & \breve{\xi}_k, \in \partial\hat{T}, \end{cases} \tag{6}$$

where

$$\vec{f}_{num} \cdot n = h \tag{7}$$

with n as the outward normal on $\partial \hat{T}$ and h as a standard numerical flux function like the Roe flux or the Lax-Friedrichs flux. Note that the flux function is approximated componentwise to one degree higher than the solution function. This is to ensure that the divergence of the flux will be a polynomial of degree m. The number of degrees of freedom is thus

$$2N_{m+1} = (m+2)(m+3). \tag{8}$$

The divergence of the flux function in the finite dimensional polynomial space is given as

$$\left(\nabla^\xi \cdot \vec{f}_h\right)(\xi) = \sum_{k=1}^{N_{m+1}} \left(\nabla^\xi \hat{l}_k\right)(\xi) \cdot \vec{f}_k. \tag{9}$$

The Spectral Difference scheme can now be written for each degree of freedom of the solution function in each cell i as

$$\frac{du_j^{(i)}}{dt} + \frac{1}{|J^{(i)}|} \sum_{k=1}^{N_{m+1}} \left(\nabla^\xi \hat{l}_k\right) \left(\hat{\xi}_j\right) \cdot \vec{f}_k^{(i)} = 0, \quad j = 1, ..., N_m, \quad i = 1, ..., N_T. \tag{10}$$

As mentioned in Section I, the above Spectral Difference scheme was found unconditionally linearly unstable for triangles.[11]

III.   The Spectral Difference Scheme for Triangles Using Raviart-Thomas Elements

The same hyperbolic Eq. (2) is considered in the reference domain. The solution function is approximated as in Eq. (3), which is the same as in the standard Spectral Difference scheme. For the flux interpolation, vector valued interpolation is used where the interpolation functions are vectors in the Raviart-Thomas (RT) space. For a degree m, the RT space is defined as

$$RT_m = (P_m)^2 + (x, y)^T P_m. \tag{11}$$

For $m = 1$, the monomials $\vec{\phi}_n$, $n = 1, ..., 8$ which form a basis in the RT space are given as $\{(1, 0)^T, (x, 0)^T, (y, 0)^T, (0, 1)^T, (0, x)^T, (0, y)^T, (x^2, yx)^T, (xy, y^2)^T\}$. Since RT_m is the smallest space having divergence in P_m,[13] it reduces the number of degrees of freedom needed for flux interpolation and hence the computational cost is reduced compared to that for the traditional Spectral Difference scheme. In 2D, the number of degrees of freedom to represent a vector-valued function in the RT space is given by

$$N_m^{RT} = (m+1)(m+3). \tag{12}$$

The flux function in the reference domain, which is defined as $|J|J^{-1}\vec{f}$, is approximated to $\vec{f}_h$ in the RT space as

$$\vec{f}_h(\xi) = \sum_{k=1}^{N_m^{RT}} f_k \vec{\psi}_k(\xi), \tag{13}$$

where $\vec{\psi}_k$, $k = 1, ... N_m^{RT}$ are interpolation functions which form a basis in the Raviart-Thomas space. Note that the basis functions are vectors and the coefficients are scalars unlike the standard Spectral Difference where the basis is scalar and the coefficients are vectors. Further, these interpolation functions have the property $\vec{\psi}_j\left(\breve{\xi}_k\right) \cdot s_k = \delta_{jk}$, where $\breve{\xi}_k$, $k = 1, ... N_m^{RT}$ are the flux collocation points and s_k are the unit vectors defined at those points. For a degree m, according to standard theory,[13] there should be $m+1$ points on each edge of the triangle and the remaining $N_m^{RT} - 3(m+1)$ in the interior. The degrees of freedom for the flux interpolation are given as

$$f_k = \begin{cases} |J|J^{-1}\vec{f}\left(\breve{\xi}_k\right) \cdot s_k & , \breve{\xi}_k \in \hat{T} \\ h & , \breve{\xi}_k \in \partial\hat{T}, \end{cases} \tag{14}$$

American Institute of Aeronautics and Astronautics

where h is a standard numerical flux. Note that the numerical flux is directly used as the degree of freedom on the boundary unlike the standard Spectral Difference where the numerical flux is used to replace the normal component of the analytical flux and is then projected into orthogonal directions to obtain the degrees of freedom.[1] To calculate the flux values, $\vec{f}$, at the flux collocation points, $\check{\xi}_k$, we have to find the solution values at those points. This is done by using a transfer matrix which is explained in Appendix A. The divergence of the flux function at the solution nodes is given as

$$\left(\nabla^\xi \cdot \vec{f}_h\right)\left(\hat{\xi}_j\right) = \sum_{k=1}^{N_m^{RT}} f_k \left(\nabla^\xi \cdot \vec{\psi}_k\right)\left(\hat{\xi}_j\right), \quad j = 1, ..., N_m. \tag{15}$$

The values of $\left(\nabla^\xi \cdot \vec{\psi}_k\right)\left(\hat{\xi}_j\right)$ can be written in the form of a matrix called differentiation matrix. The evaluation of the differentiation matrix is given in Appendix B. The new Spectral Difference scheme can now be written for each degree of freedom of the solution function in each cell i as

$$\frac{du_j^{(i)}}{dt} + \frac{1}{|J^{(i)}|} \sum_{k=1}^{N_m^{RT}} f_k^{(i)} \left(\nabla^\xi \cdot \vec{\psi}_k\right)\left(\hat{\xi}_j\right) = 0, \quad j = 1, ..., N_m, \quad i = 1, ..., N_T. \tag{16}$$

The above equation is rewritten in terms of the residual, R, as

$$\frac{dU}{dt} = R(U), \tag{17}$$

where $U = (u_1^{(1)}, u_2^{(1)}, ..., u_{N_m}^{(N_T)})^T$ comprises all solution degrees of freedom in all the cells.

IV. Time Integration

IV.A. TVD Runge-Kutta Time Discretization

For time-dependent problems, higher order explicit multistage Runge-Kutta schemes by Gottlieb and Shu[14] which preserve the TVD property of the spatial operator are used to integrate the system of ODEs (17). We use the Runge-Kutta schemes, where the solution at $(n+1)$-th iteration, U^{n+1}, is obtained from U^n as follows.

$$w^{(0)} = U^n,$$

$$w^{(k)} = \sum_{l=0}^{k-1} \alpha_{kl} w^{(l)} + \Delta t \beta_{kl} R^{(l)} \quad k = 1, ..., p,$$

$$U^{n+1} = w^{(p)}, \tag{18}$$

where p is the number of intermediate stages, Δt is the time step and $R^{(l)}$ is the residual evaluated at $w^{(l)}$. Note that the bracketed superscript here stands for different stages and not for different cells. For a 3 stage ($p = 3$) 3rd order TVD Runge-Kutta scheme (Shu-RK3), the coefficients are given in matrix form as

$$\alpha = \begin{bmatrix} 1 & & \\ \frac{3}{4} & \frac{1}{4} & \\ \frac{1}{3} & 0 & \frac{2}{3} \end{bmatrix}, \quad \beta = \begin{bmatrix} 1 & & \\ 0 & \frac{1}{4} & \\ 0 & 0 & \frac{2}{3} \end{bmatrix}. \tag{19}$$

Here (l, k) represents the index to the matrix elements with $l = 0, ..., k-1$ and $k = 1, ..., p$. And for a 2 stage, 2nd order scheme (Shu-RK2), the coefficients are given as

$$\alpha = \begin{bmatrix} 1 & \\ \frac{1}{2} & \frac{1}{2} \end{bmatrix}, \quad \beta = \begin{bmatrix} 1 & \\ 0 & \frac{1}{2} \end{bmatrix}. \tag{20}$$

American Institute of Aeronautics and Astronautics

IV.B. Strong Stability Preserving Time Discretization

Following the successful application of TVD Runge-Kutta schemes for hyperbolic partial differential equations, a new general class of Strong Stability Preserving (SSP) schemes was developed by Gottlieb and Shu.[15] SSP schemes, in general, maintain stability in the same norm as that of the first-order forward Euler discretization, at potentially higher orders of temporal accuracy, or larger permissible time steps. The TVD Runge-Kutta scheme is one type of SSP scheme, where the stability is preserved with respect to the Total Variation norm. More efficient SSP schemes have been developed by Spiteri and Ruuth.[16] Such a 5 stage 4th order SSP scheme is also used in our linear stability analysis of the RT schemes. The coefficients are given in the matrix form as

$$
\alpha = \begin{bmatrix}
1 & & & & \\
0.444370494067 & 0.555629505933 & & & \\
0.620101851385 & 0 & 0.379898148615 & & \\
0.178079954108 & 0 & & 0.821920045892 & \\
0.006833258840 & 0 & 0.517231672090 & 0.127598311333 & 0.348336757737
\end{bmatrix}, \tag{21}
$$

$$
\beta = \begin{bmatrix}
0.391752227004 & & & & \\
0 & 0.368410592630 & & & \\
0 & 0 & 0.251891774247 & & \\
0 & 0 & 0 & 0.544974750212 & \\
0 & 0 & 0 & 0.084604163382 & 0.226007483194
\end{bmatrix}. \tag{22}
$$

IV.C. Implicit Time Discretization

The time discretization can be written in a backward Euler form as

$$
\frac{U^{n+1} - U^n}{\Delta t} = R(U^{n+1}), \tag{23}
$$

where the residual R is defined in Eqns. (16), (17). The residual is now expanded in Taylor series as follows

$$
R(U^{n+1}) = R(U^n) + \frac{dR(U^n)}{dt}\Delta t + ... \tag{24}
$$

We can also write the derivative term in the above equation as

$$
\frac{dR(U^n)}{dt}\Delta t = \frac{dR(U^n)}{dU}\frac{dU}{dt}\Delta t \simeq \frac{dR(U^n)}{dU}(U^{n+1} - U^n). \tag{25}
$$

If we denote $(U^{n+1} - U^n)$ as ΔU^n, the implicit scheme now reduces to

$$
\left(I - \Delta t\frac{dR(U^n)}{dU}\right)\Delta U^n = \Delta t R(U^n), \tag{26}
$$

where $\frac{dR(U)}{dU}$ is the Jacobian matrix of the residual vector. The above linear system of equations at each time step has to be solved to get ΔU^n and hence the solution U^{n+1}. We use implicit methods in particular for steady problems, where we require no time accuracy, but rather large times steps. Note that as $\Delta t \to \infty$, we obtain Newton iterations. The iterations of the above form with finite value for Δt can be interpreted as damped Newton iterations.

V.   Linear Stability Analysis

The new variant of the Spectral Difference scheme which uses Raviart-Thomas elements has been subject to a linear stability analysis by May,[12] which is extended here. The analysis is carried out for a simplified setup, using a Cartesian mesh with every cell subdivided into two triangles, and considering a limited range of advection velocities. While a more general analysis is certainly possible, in particular considering skewed meshes, the standard Spectral Difference Scheme of third (and presumably higher) order already fails in this setting, while we demonstrate in this section that the new formulation proves stable.

We consider the two-dimensional linear advection

$$\frac{\partial u}{\partial t} + \nabla \cdot \vec{f}(u) = 0, \tag{27}$$

with $\vec{f}(u) = (c_1 u, c_2 u)$, where $c_1 = |c|cos\theta, c_2 = |c|sin\theta$ for the advection angle $\theta \in [0, \pi/2]$ and $|c|$ being the magnitude of advection velocity, in a rectangular domain with periodic boundary conditions. A Cartesian mesh is created and each mesh element, identified by (i, j), is subdivided into two triangular elements. The Spectral Difference scheme based on RT elements is then formulated for these triangular elements. A similar, but more general, analysis has been used in[11] to demonstrate linear instability of the classical SD scheme. The SD formulation in semi-discrete form, using upwind fluxes on the boundary of the elements, is given as

$$\Delta t \dot{U}^{(i,j)} = -\nu \left(AU^{(i,j)} + BU^{(i-1,j)} + CU^{(i,j-1)} \right), \tag{28}$$

where $U = (u_1, u_2, ..., u_{2N_m})^T$ comprises all solution degrees of freedom in the Cartesian mesh element (i, j). The CFL number is given as $\nu = \frac{|c|\Delta t}{h}$, where h is the Cartesian mesh edge length. A, B and C are matrices resulting from the concatenated application of the transfer matrix (see Appendix A), used to evaluate the solution at flux collocation nodes, the application of upwind fluxes, and the differentiation matrix (see Appendix B), to evaluate the divergence of flux at solution collocation nodes. The analysis considered here is based on linear stability analysis for periodic problems.[17] The solution variable is initialized with a periodic function. The variable is then decomposed into different frequency modes by Fourier transformation and the behavior of these individual modes is analyzed. If $\hat{U}e^{i(k_x x + k_y y)}$ is one particular mode with k_x, k_y being the wave numbers in x and y directions, respectively, then the SD discretization for this mode will take the form

$$\Delta t \frac{d\hat{U}}{dt} = \nu Z \hat{U}, \tag{29}$$

where $Z = -\left(A + Be^{-i\sigma} + Ce^{i\kappa} \right)$ is the Fourier symbol of the spatial discretization, and $(\sigma, \kappa) = (k_x h, k_y h)$ defines the grid frequency. The numerical stability of Eq. (29) depends on the eigensystem of matrix Z. The above linear system of equations (Eq. (29)) can be decoupled by diagonalizing Z. If H denotes the matrix whose elements are the eigenvectors of Z and $\lambda_j, j = 1, ..., jmax$ are the corresponding eigenvalues, then the similarity transformation can be written as

$$Z = H\Lambda H^{-1}, \tag{30}$$

where $\Lambda = diag(\lambda_1, ..., \lambda_{jmax})$. This transformation gives a set of independent scalar equations of the form

$$\frac{dw_j}{dt} = \lambda_j w_j, \tag{31}$$

where $Hw = \hat{U}$ and w is the vector whose elements are the new scalar variables w_j. The solution to Eq. (31) takes the form:

$$w_j(t) = w_j(0)exp(\lambda_j t). \tag{32}$$

From the above equation, it is clear that, for the solution w_j to be bounded, the real part of λ_j should be non-positive.

V.A. Linear Stability Analysis for the Spatial Discretization

Linear stability analysis is done to find the position of flux nodes for which the scheme is linearly stable. The eigenvalues λ of Z are evaluated numerically at discrete grid frequencies $(\sigma, \kappa) \in [0, 2\pi]^2$. For spatially stable discretization, all the eigenvalues of Z should have non-positive real part. For RT_k elements we have $k + 1$ nodes on each edge of the triangle,[13] while remaining degrees of freedom are located in the interior. We place edge nodes at Legendre-Gauss quadrature points.[18] It has been found that the placement of flux nodes on the edges does not affect the linear stability properties for RT_1, RT_2 and RT_3 schemes, whereas the flux node placement in the interior of the triangle has considerable effects. As mentioned in section III, degrees of freedom for the flux function are determined by using both flux nodes and a unit vector at those flux nodes. Here the interior flux points are chosen such that one point with two mutually orthogonal unit vectors form two flux nodes, which means two degrees of freedom at each point. For RT_1, the two interior

degrees of freedom are put at the centroid and this was found to be stable. In the case of RT_2, there are six interior degrees of freedom (three points). The position of these three points can be varied linearly by a scaling parameter α, such that when $\alpha = 1$ the three points coincide with the corner points and when $\alpha = 0$ the three points collapse onto the centroid of the triangle. Both $\alpha = 1$ and $\alpha = 0$ are excluded since those configurations lead to singular stencils. If ξ_i^e, $i = 1, 2, 3$ are the 3 vertices of the reference triangle and ξ^c is the centroid, then the linear variation of the interior flux points ξ_i can be written in the form

$$\xi_i = \xi^c + \alpha(\xi_i^e - \xi^c), \quad i = 1, 2, 3. \tag{33}$$

The maximum eigenvalue of Z is found numerically, considering sufficiently many grid frequencies (σ, κ) and advection angles θ, for different values of α. Even though Eq. (28) is valid for all $\theta \in [0, \frac{\pi}{2}]$, we consider only $\theta \in [0, \frac{\pi}{4}]$ due to symmetry. Fig. 1 shows the maximum value of the real part of the eigenvalues (λ) of Z for different values of the scaling parameter. For $\alpha < 0.5$, the discretization is unstable for all advection angles as the real part of the eigenvalues is positive for all angles. This unstable region, where there is positive real part for the eigenvalues can be observed in the plot as well. Though a stable region can be inferred from the plot for $\alpha \geq 0.5$, there is a region of instability for advection angles close to zero for a range of values of the scaling parameter α, which is not so obvious from the plot due to low resolution. This unstable region, where the eigenvalues have very low magnitude positive real part, is shown in Fig. 2 which has a higher resolution. From the numerical analysis it is found that, if we consider all possible advection angles, the discretization is stable for all advection angles only for $0.5 \leq \alpha < 0.521$.

The maximum spectral radius of Z, taken over all grid frequencies, is also calculated and is plotted for
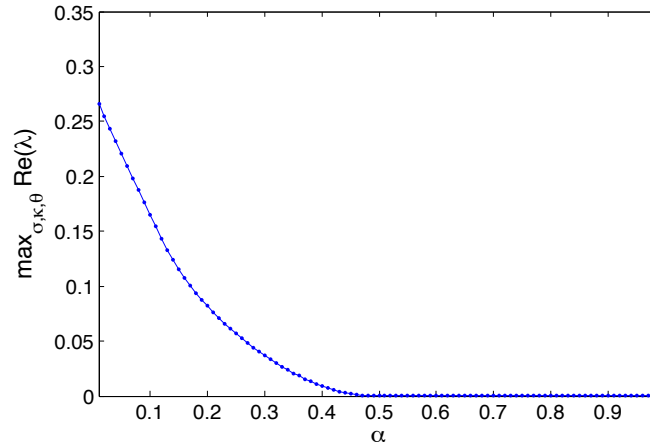

Figure 1. *Influence of the scaling parameter α on the spectrum of the Fourier symbol Z for the RT_2-based Spectral Difference scheme*

different advection angles and scaling parameters (Fig. 3). As shown in the plot, the spectral radius increases with the scaling parameter for all advection angles. Considering the fact that the smallest spectral radius is desirable to get the maximum stable CFL number for time integration, and the above observations on the region of stability, $\alpha = 0.5$ seems to be the optimal choice for flux node placement for RT_2 discretization. Interestingly, this optimal choice corresponds to using a high-order integration rule in the interior of triangles, which is exact for polynomials of total degree 2. Similar linear stability analysis[11] showed that the 3rd order traditional Spectral Difference scheme failed in having a stable flux-point distribution, unlike the 3rd order (RT_2) RT-based Spectral Difference scheme.

For RT_3, different sets of interior points obtained by varying α did not give any stable discretization. However, it was found that using the points of a six-point quadrature rule[12] results in eigenvalues with non-positive real parts. Motivated by the finding of such a stable configuration, a stability analysis has been done to choose the flux points using two scaling parameters α and β. Out of the 6 interior degrees of freedom, 3 are varied using α and the other 3 are varied using β as follows. If ξ_i^e, $i = 1, 2, 3$ are the 3 vertices of the reference triangle, ξ_i^e, $i = 4, 5, 6$ are the points on the middle of each edge of the reference
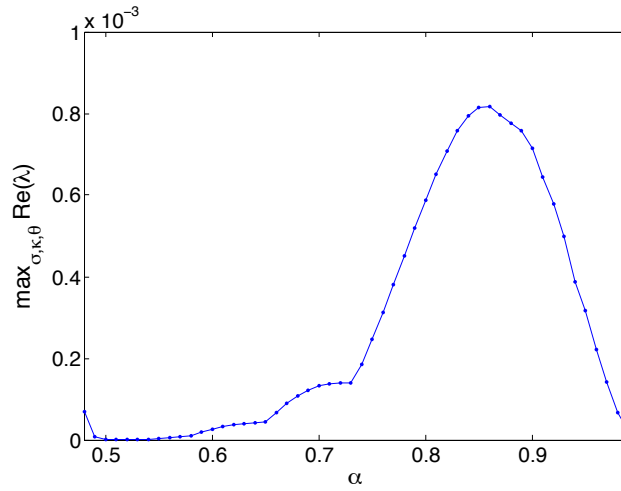
American Institute of Aeronautics and Astronautics

Figure 2. *Influence of the scaling parameter α on the spectrum of the Fourier symbol Z for the RT_2-based Spectral Difference scheme*
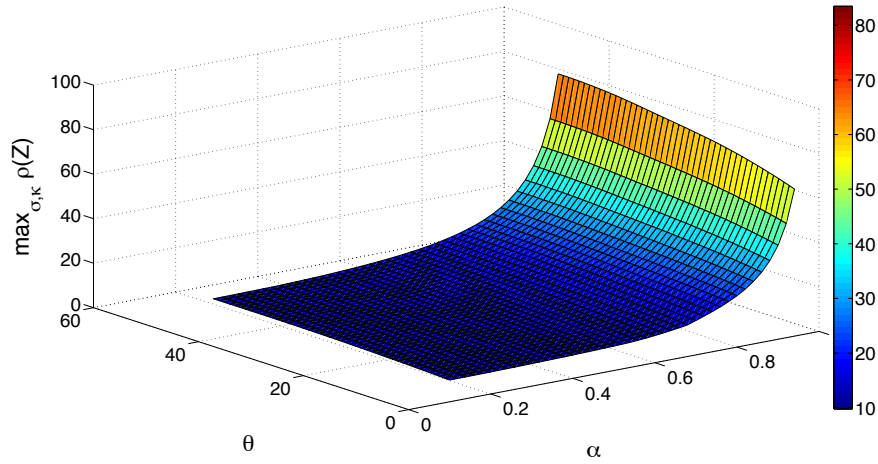

Figure 3. *Influence of the scaling parameter α and the advection angle θ (in degrees) on the maximum spectral radius of the Fourier symbol Z for the RT_2-based Spectral Difference scheme*

triangle, and ξ^c is the centroid, then the position of the six interior flux points ξ_i is varied as

$$\xi_i = \xi^c + \alpha(\xi_i^e - \xi^c), \quad i = 1, 2, 3,$$
$$\xi_i = \xi^c + \beta(\xi_i^e - \xi^c), \quad i = 4, 5, 6. \tag{34}$$

A stable region was found numerically using the above two-parameter scaling, for $\theta \in [0, \frac{\pi}{4}]$, and is shown in Fig. 4. The shaded region corresponds to the stable region where the eigenvalues are non-positive for *all* considered advection angles. The parameter values corresponding to the six-point quadrature rule are highlighted in Fig. 4 by a circle. Numerically it was found that the maximum spectral radius of Z monotonically increases with both α and β. Fig. 5 shows an example for $\theta = \frac{\pi}{8}$. Numerical evaluation of the spectral radius supports the conjecture that the optimal configuration in the stable region, where the spectral radius is minimum, is actually that obtained by the six-point quadrature rule, although due to finite resolution of the parameter values and advection angles in this study this cannot be explicitly proven.

Fig. 6 shows the flux node distribution used for RT_1, RT_2 and RT_3 schemes we have used in the present paper. On the edges, the nodes are placed at the Gauss-Legendre quadrature points.[18] Interior points in the RT_2 element correspond to $\alpha = 0.5$ and those in the RT_3 element correspond to the points obtained using the six-point quadrature rule. Fig. 7 shows the spectrum of the Fourier symbol (Z) for the optimal
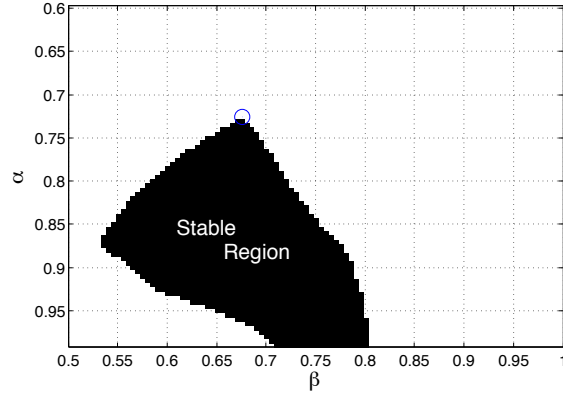
American Institute of Aeronautics and Astronautics

Figure 4. *Influence of the scaling parameters α and β on stability of the RT_3-based Spectral Difference scheme. Blue circle, which lies inside the stable region, corresponds to the point obtained using six-point quadrature rule.*
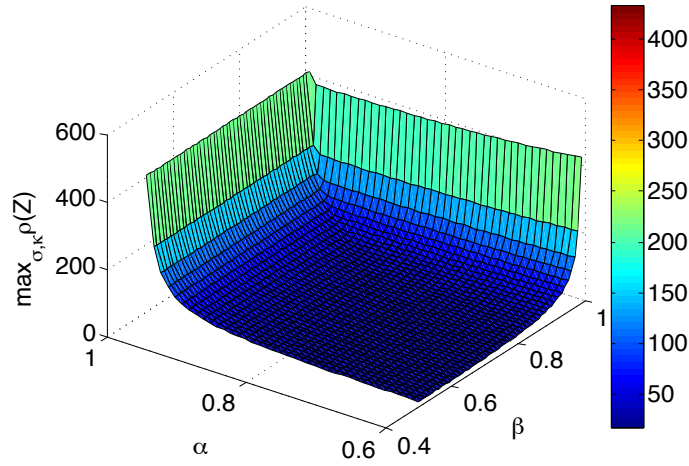

Figure 5. *Influence of the scaling parameters α and β on the maximum spectral radius of the Fourier symbol Z for the RT_3-based Spectral Difference scheme for $\theta = \frac{\pi}{8}$*

and stable choice of flux nodes for RT_m, $m = 1, 2, 3$ elements for the advection angle $\theta = 45$ degree.

V.B.   Linear Stability Analysis for the Full Discretization

Different explicit multistage time discretization methods are used for the time derivative term in Eq. (29). The stable flux points shown in Fig. 6 are used here for the linear stability analysis for the full discretization. The amplification factor G, such that $\hat{U}^{n+1} = G\hat{U}^n$, depends on parameters such as the advection angle θ, the grid frequencies (σ, κ) and the CFL number ν. Using Eq. (18), $\hat{U}^{n+1}$ is obtained as

$$
\begin{aligned}
w^{(0)} &= \hat{U}^n, \\
w^{(k)} &= \sum_{l=0}^{k-1} \alpha_{kl} w^{(l)} + \nu \beta_{kl} Z w^{(l)} \qquad k = 1, ..., p, \\
\hat{U}^{n+1} &= w^{(p)}.
\end{aligned} \tag{35}
$$

If $G^{(k)}$ is the amplification matrix in the k-th intermediate step, then one obtains

$$
G^{(0)} = I, \qquad G^{(k)} = \sum_{l=0}^{k-1} \left(\alpha_{kl} I + \nu \beta_{kl} Z \right) G^{(l)} \qquad k = 1, ..., p.
$$

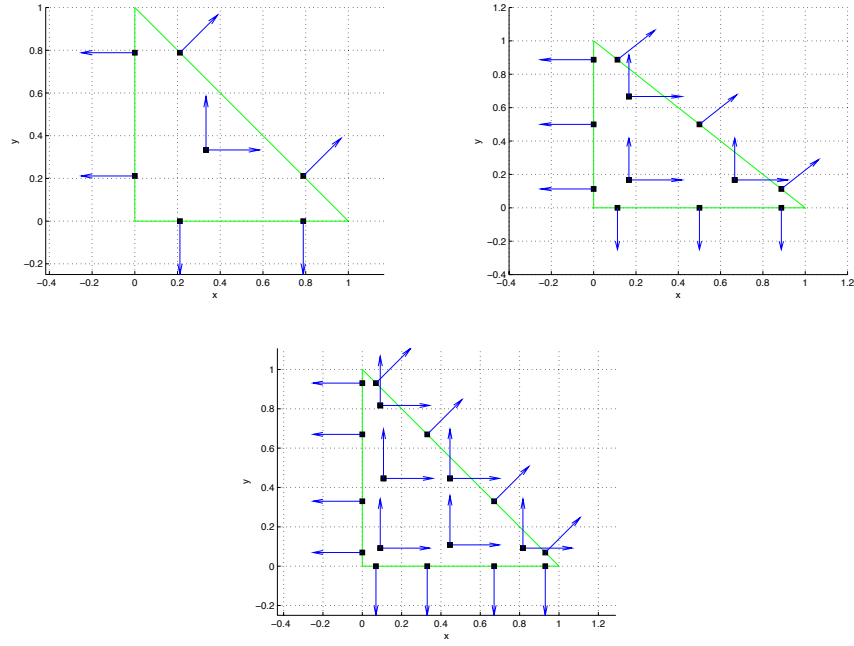American Institute of Aeronautics and Astronautics

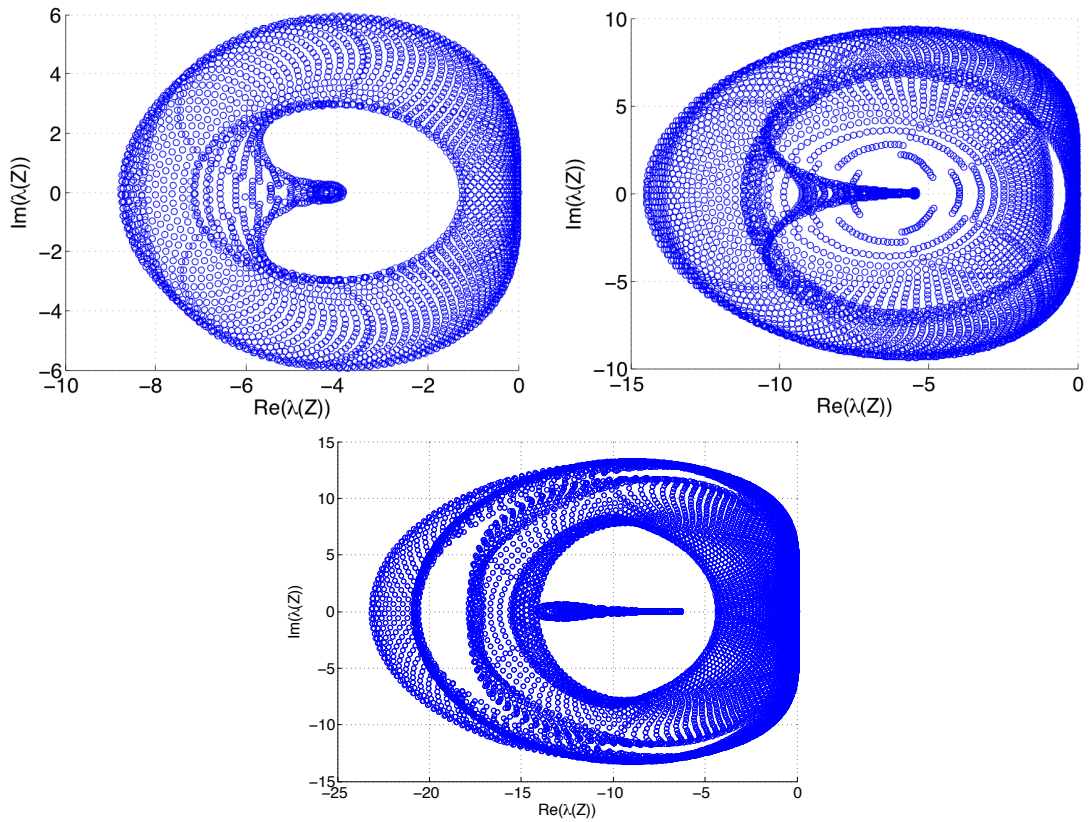**Figure 6.** *RT1 (top left), RT2 (top right) and RT3 (bottom) Elements*

Figure 7. *Spectrum of the Fourier symbol (Z) for the optimal and stable choice of flux nodes for RT1 (top left), RT2 (top right) and RT3 (bottom) elements for the advection angle $\theta = 45°$*

American Institute of Aeronautics and Astronautics

$G = G^{(p)}$ is the amplification matrix for the update from U^n to U^{n+1}. For a stable discretization, it is sufficient to have $\parallel G \parallel \leq 1$, where $\parallel G \parallel$ is any p-norm. In that case the $\hat{U}$ vector will remain bounded over iterations, for a bounded initial vector. It is sufficient to have $\rho \leq 1$, where ρ is the spectral radius of G. In other words, for a stable time and space discretization, all the eigenvalues of G must lie inside the unit circle in the complex plane. We get the maximum allowable CFL numbers by requiring that $\rho \leq 1$. Here ρ is taken as the maximum eigenvalue found from sufficiently many grid frequencies (σ, κ). The maximum allowable CFL numbers for different time discretization methods are found numerically for different values of advection angles θ.

It was observed that, for both RT_2 and RT_3 schemes, Shu-RK2 time discretization (Eqns. (18) and (20)) is unstable for certain advection angles. Both the Shu-RK3 scheme, (Eqns. (18) and (19)), and the 5-stage 4th order SSP scheme (Eqns. (18), (21) and (22)), are stable under a CFL condition for all advection angles. Tables 1 and 2 show the maximum stable CFL numbers for a few advection angles. The spectrum of G for a (stable) CFL number of 0.170 for $\theta = 45°$ using Shu-RK3 time stepping on RT_2 discretization is shown in Fig. 8(a). Figure 8(b) shows the spectrum for the same at unstable CFL number of 0.175. The spectrum of G for a CFL number of 0.125 for $\theta = 45°$ using Shu-RK2 time stepping on RT_2 discretization is shown in Fig. 9(a). A close view near the right edge of the unit circle as shown in Fig.9(b) shows that there are certain unstable modes which lie outside the unit circle. This situation, in fact, occurs for all CFL numbers and it makes the Shu-RK2 time stepping unstable.   The CFL numbers for Shu-RK3 and SSP 4th order for RT_2

Table 1. CFL number when Shu-RK3 scheme is used for RT_m $(m = 1, 2$ and $3)$ elements

RT_m	$\theta = 0$	$\theta = \pi/8$	$\theta = \pi/4$
RT_1	0.352	0.289	0.281
RT_2	0.215	0.182	0.172
RT_3	0.140	0.118	0.108

Table 2. CFL number when 4th order SSP scheme is used for RT_m $(m = 1, 2$ and $3)$ elements

RT_m	$\theta = 0$	$\theta = \pi/8$	$\theta = \pi/4$
RT_1	0.564	0.462	0.440
RT_2	0.337	0.289	0.281
RT_3	0.223	0.194	0.185

(a) *Spectrum of G for CFL = 0.170*

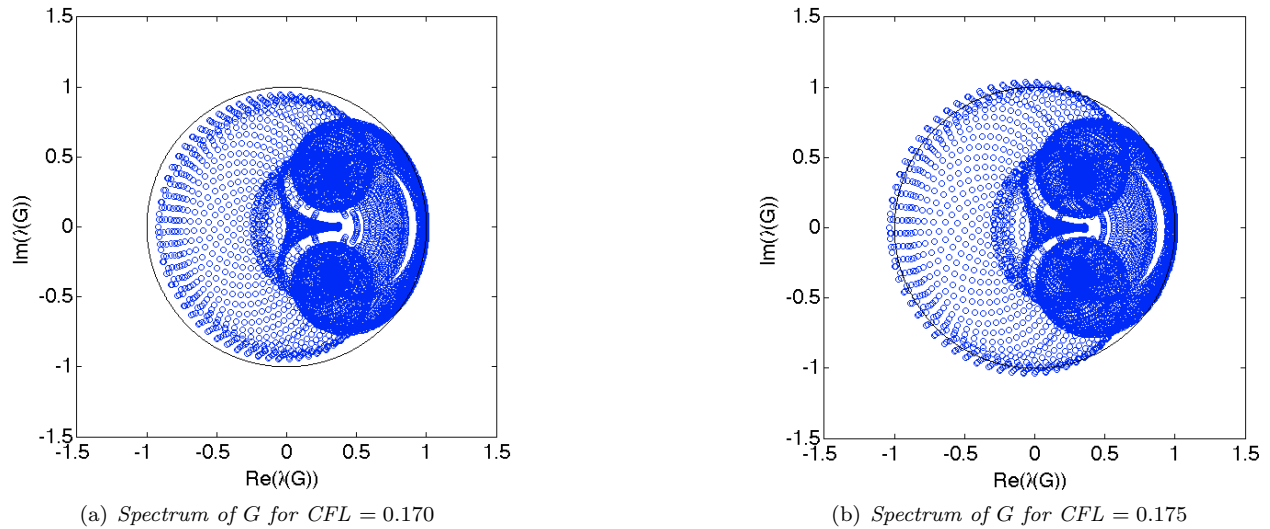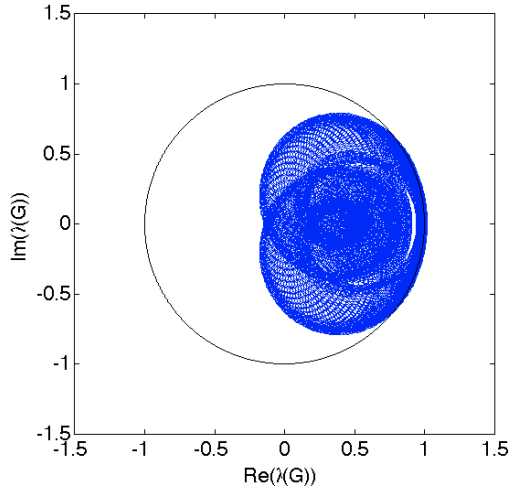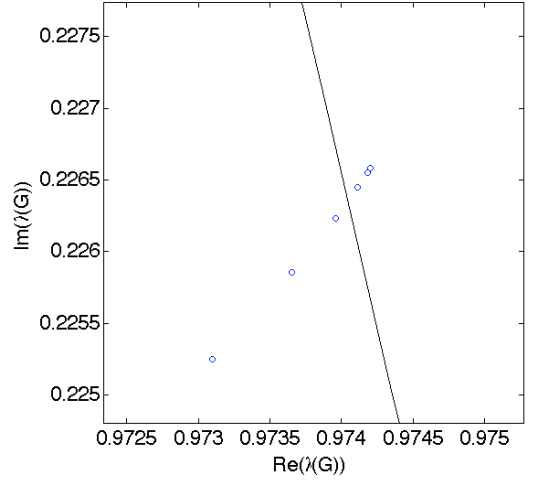(b) *Spectrum of G for CFL = 0.175*

Figure 8. *Spectrum of G for different CFL numbers for $\theta = 45°$ using Shu-RK3 time stepping on RT_2 discretization*

American Institute of Aeronautics and Astronautics

(a) *Spectrum of G for CFL = 0.125*

(b) *Close view of the spectrum of G for CFL = 0.125*

Figure 9. *Spectrum of G for different CFL numbers for $\theta = 45°$ using Shu-RK2 time stepping on RT_2 discretization*

discretization are also plotted in Fig. 10(a). The CFL numbers for the SSP 4th order scheme are roughly 1.6 times those of the Shu-RK3. Fig. 10(b) shows the CFL number normalized with the number of stages which are 3 for Shu-RK3 and 5 for SSP 4th order. From the figure, it is clear that the computational effort for both of these time discretization is same as the two curves lie close. However, SSP 4th order scheme has got one order of accuracy higher than the Shu-RK3. So the SSP 4th order scheme can be considered to have superior performance compared to Shu-RK3.
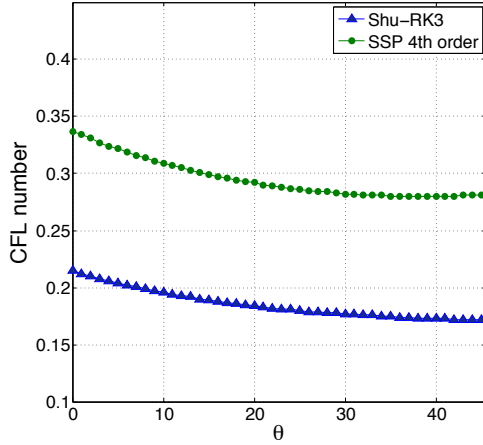
(a) *CFL number vs. Advection angle*
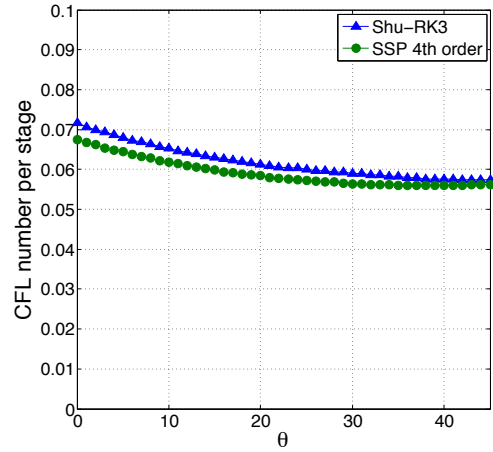
(b) *CFL number per stage vs. Advection angle*

Figure 10. *Influence of CFL number on different advection angles for Shu-RK3 and the 4th order SSP time stepping schemes*

VI. Convergence Study: 2D Linear Advection Problem

Numerical simulations using the new Spectral Difference scheme have been performed to solve the linear advection Eq. (27) with $\vec{f}(u) = (c_x u, c_y u)$, where c_x and c_y are the advection velocities in the x and y directions, respectively. The equation is solved for a rectangular domain, $[-1, 1] \times [-1, 1]$, with periodic boundary conditions. The solution field has been initialized at $t = 0$ as $u(x, y) = sin(2\pi(x + y))$. A convergence study has been conducted using different mesh sizes for the RT_m-based Spectral Difference discretization, where $m = 1, 2$ and 3. The flux nodes in the reference element are distributed as shown in

American Institute of Aeronautics and Astronautics

Fig. 6. The advection velocities considered were $c_x = cos(\frac{\pi}{8})$ and $c_y = sin(\frac{\pi}{8})$. The upwind flux was used as the numerical flux at the cell interfaces. Time integration was done using Shu-RK3 scheme. The numerical results were compared with the exact analytic solution which at any time t is given as

$$u(x, y, t) = u(x - c_x t, y - c_y t, 0). \tag{36}$$

Fig. 11 shows the l_∞ error at $t = 0.1$ for different mesh (N) and RT elements in logarithmic scale, where $N = \frac{2}{h}$ with h as the characteristic length of the mesh. Tables 3, 4 and 5 show l_∞ errors and orders of
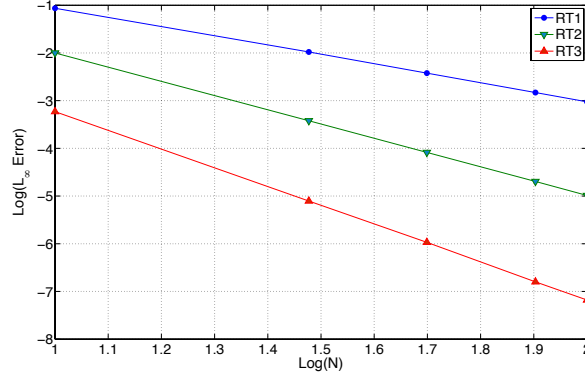

Figure 11. *Convergence plot: The variation of l_∞ error with different mesh (N) and RT elements in logarithmic scale.*

accuracy for different meshes and RT elements. The order of accuracy achieved here for the RT_m scheme is approximately $m + 1$, the optimal attainable order for smooth solutions.

Table 3. **Order of accuracy and the l_∞ error for different meshes for RT_1 discretization**

N	l_∞ error	Order of accuracy
10	8.64E-2	
30	1.05E-2	1.9184
50	3.78E-3	1.9999
80	1.48E-3	1.9950
100	9.47E-4	2.0009

Table 4. **Order of accuracy and the l_∞ error for different meshes for RT_2 discretization**

N	l_∞ error	Order of accuracy
10	1.00E-2	
30	3.79E-4	2.9790
50	8.23E-5	2.9896
80	2.02E-5	2.9887
100	1.03E-5	3.0184

VII.   Numerical Experiments: 2D Euler Equations

We consider the 2D steady Euler equations in the conservative form as

$$\frac{\partial \mathbf{f}(\mathbf{u})}{\partial x} + \frac{\partial \mathbf{g}(\mathbf{u})}{\partial y} = 0, \tag{37}$$

American Institute of Aeronautics and Astronautics

N	l_∞ error	Order of accuracy
10	5.88E-4	
30	7.86E-6	3.9276
50	1.07E-6	3.9037
80	1.59E-7	4.0564
100	6.61E-8	3.9335

where $\mathbf{u}$, $\mathbf{f}$ and $\mathbf{g}$ are given by

$$\mathbf{u} = \begin{bmatrix} \rho \\ \rho u \\ \rho v \\ E \end{bmatrix} \quad \mathbf{f} = \begin{bmatrix} \rho u \\ \rho u^2 + p \\ \rho u v \\ u\,(E + p) \end{bmatrix} \quad \mathbf{g} = \begin{bmatrix} \rho v \\ \rho u v \\ \rho v^2 + p \\ v\,(E + p) \end{bmatrix}, \quad (38)$$

where ρ is the density of the fluid, u is the x velocity, v is the y velocity, p is the pressure, and E is the total energy. To close the system of equations, we assume the ideal gas for which the relation between pressure and energy is given as

$$p = (\gamma - 1)\left(E - \frac{1}{2}\rho\left(u^2 + v^2\right)\right), \quad (39)$$

where γ is the specific heat capacity ratio and is 1.4 for air.

The Euler Eqns. (37) and (38) have been solved numerically on an unstructured grid for the subsonic steady-state flow over the airfoil NACA0012 using the newly formulated RT-based Spectral Difference scheme. The surface of the airfoil is approximated by cubic splines. The simulations were done using 2nd order (RT_1), 3rd order (RT_2) and 4th order (RT_3) schemes. The flux nodes in the reference element are distributed as shown in Fig. 6. The computational mesh (1440 elements) used for the simulation is shown in Fig. 12. The solution field has been initialized in such a way that both non-dimensional pressure p and
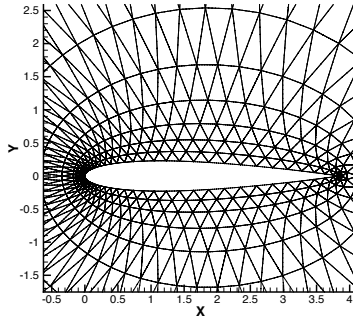

Figure 12. *Computational mesh (1440 elements)*

density ρ have value one in the entire domain. The initial values of other solution variables are found from the free stream Mach number M_∞ and the angle of attack α. Slip boundary condition has been used on the surface of the airfoil and free stream values on the outer boundary. Jameson's H-CUSP flux[19] was used as the numerical flux at the cell interfaces and it provides appropriate numerical dissipation for the test cases considered here. So far no limiters or otherwise addition of artificial diffusion has been implemented. Two test cases are presented below, each with a particular Mach number and angle of attack. In both cases, time stepping was done using the implicit scheme mentioned in section IV.C. To solve the linear system which was obtained as a result of implicit discretization, we have used the PETSc library.[20] The basic parameters to solve the linear system using an implicit scheme are the Jacobian matrix $\frac{dR(U)}{dU}$, the solution methodology and the preconditioning of the system. The assembly of the Jacobian matrix is straightforward with the transfer matrix and differentiation matrix available for residual computation. In our implementation we use

American Institute of Aeronautics and Astronautics

an exact differentiation of the residual in order to allow asymptotic quadratic convergence, once a sufficiently good solution approximation has been reached. We use a heuristic time step control in the damped Newton / backward Euler approach outlined in section IV.C, such that after a small number of start-up iterations the CFL number of the implicit scheme increases to infinity, as the residual is reduced, and at the same time the relative accuracy for solution of the linear systems is increased. Furthermore, for small CFL numbers (typically CFL < 1000), the Jacobian matrix is frozen for a number of iterations (typically 3), while for larger CFL numbers it is recomputed at each iteration. The preconditioning of the system is done using Incomplete LU (ILU) factorization,[21] typically ILU(2), and the linear system is solved using the restarted GMRES algorithm,[22] where we typically restart after 30 Krylov vectors.

VII.A. Test Case 1: Subsonic Non-Lifting Flow

Here, we consider free stream Mach number $M_\infty = 0.3$ and angle of attack $\alpha = 0°$. Fig. 13 shows the decay of the residual against number of Jacobian (Eqn. (26)) evaluations for RT_1, RT_2 and RT_3 schemes. Note
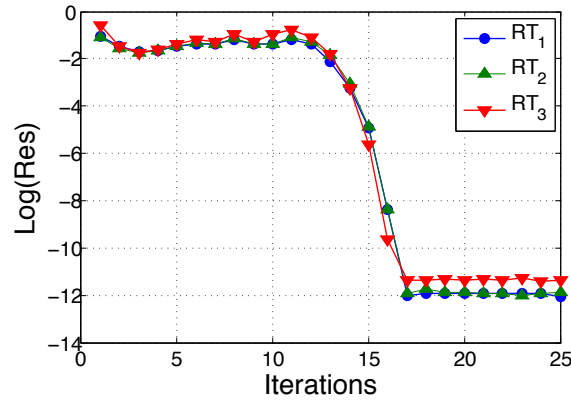

Figure 13. *Convergence of the residual for RT_1,RT_2 and RT_3 schemes for $M_\infty = 0.3$ and $\alpha = 0°$ (Residual vs. Number of Jacobian evaluations)*

that we have not attempted to optimize for run-time, but have rather used the same settings (time step control, start-up iterations, etc.) for all schemes. It is likely that convergence can be improved by adjusting parameters, although this is not our aim here. Fig. 14 shows the contours of Mach number around the airfoil generated using the RT_3 scheme. Even with a coarse mesh, the Mach contours are well captured. Note that our postprocessing renders the solution in each triangle individually, and thus the contour lines are discontinuous across mesh elements. Smooth contours are thus indicative of adequate resolution. For validation purposes, Mach number contours generated using a 4th order Discontinuous Galerkin scheme is shown along with 4th order new Spectral Difference (RT_3) in Fig. 15. As one can observe from the figure, the Mach number contours generated using the new Spectral Difference scheme are very similar to those generated using the DG method.   Fig. 16 shows the Mach number contours around the leading edge of
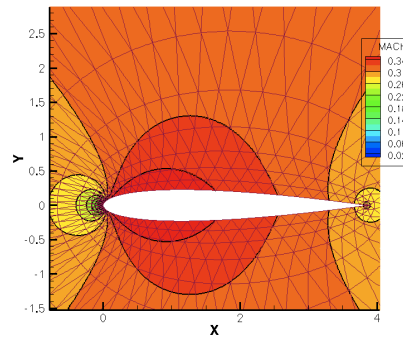

Figure 14. *Mach number contours generated using the RT_3 scheme for $M_\infty = 0.3$ and $\alpha = 0°$*

the airfoil generated using RT_1, RT_2 and RT_3 schemes. It can be observed that the Mach number contours

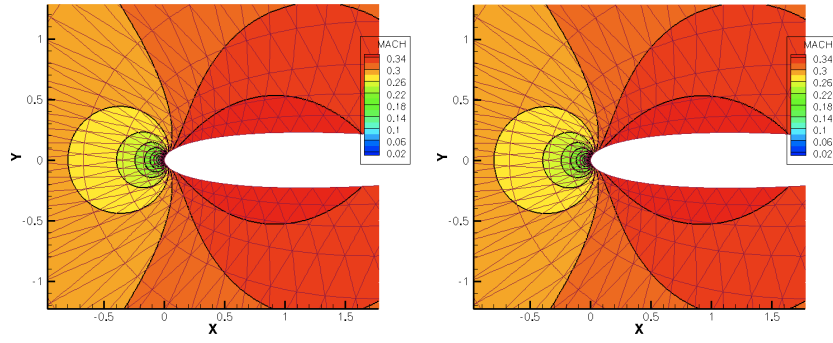American Institute of Aeronautics and Astronautics

Figure 15. *Mach number contours generated using 4th order Discontinuous Galerkin (left) and RT_3 (right) schemes for $M_\infty = 0.3$ and $\alpha = 0°$*

are better captured using the RT_3 scheme as it has got the solution with the highest polynomial degree compared to that of RT_1 and RT_2 schemes.
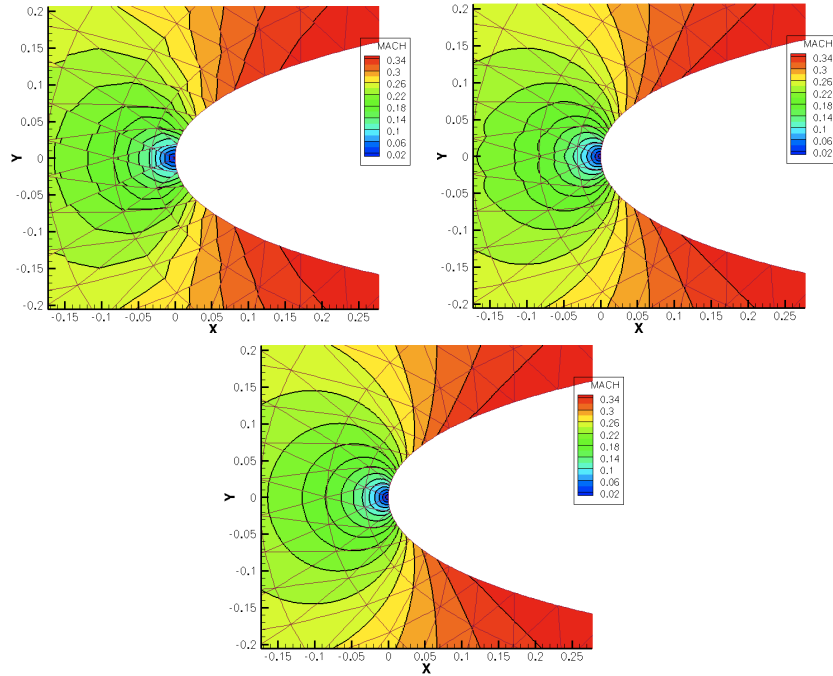

Figure 16. *Mach number contours generated using RT_1 (top left), RT_2 (top right) and RT_3 (bottom) schemes for $M_\infty = 0.3$ and $\alpha = 0°$*

VII.B. Test Case 2: Subsonic Lifting Flow

In the second test case, we consider free stream Mach number $M_\infty = 0.4$ and angle of attack $\alpha = 5°$. The computational grid used was the same as in the first test case. Fig. 17 shows the decay of the residual against number of Jacobian (Eqn. (26)) evaluations for RT_1, RT_2 and RT_3 schemes. Fig. 18 shows the contours of Mach number around the airfoil generated using the RT_3 scheme. The Mach number contours around the leading edge of the airfoil, generated using RT_1, RT_2 and RT_3 schemes are shown in Fig. 19. Like in the previous test case, the Mach number contours are smoother for RT_3 scheme compared to RT_1 and RT_2 schemes because of the higher polynomial degree for the interpolation. Mach number contours generated using 4th order DG scheme are shown along with 4th order new Spectral Difference (RT_3) in Fig. 20.
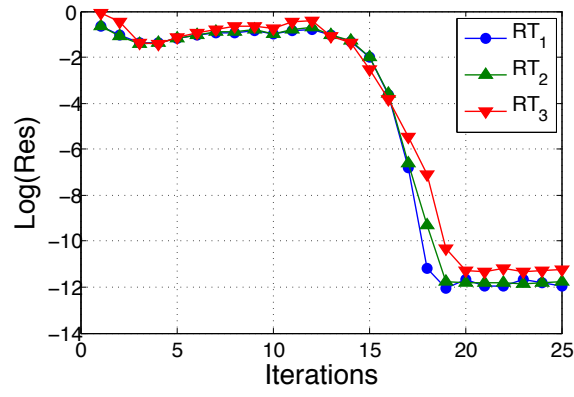
American Institute of Aeronautics and Astronautics

Figure 17. *Convergence of the residual for RT_1, RT_2 and RT_3 schemes for $M_\infty = 0.4$ and $\alpha = 5°$ (Residual vs. Number of Jacobian evaluations)*
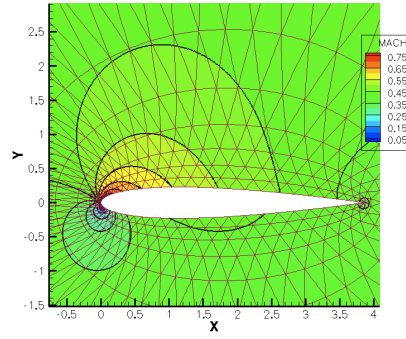

Figure 18. *Mach number contours generated using the RT_3 scheme for $M_\infty = 0.4$ and $\alpha = 5°$*
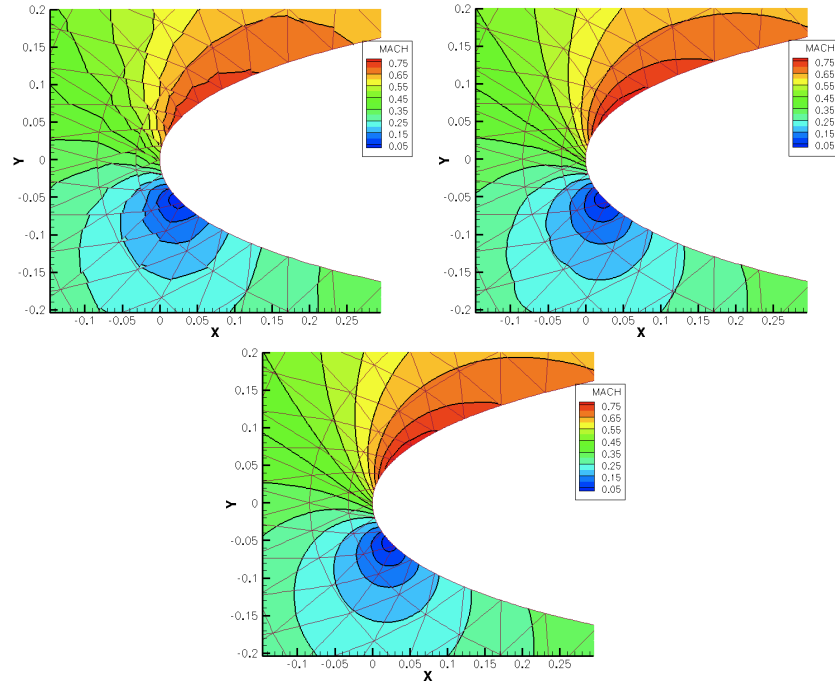

Figure 19. *Mach number contours generated using RT_1 (top left), RT_2 (top right) and RT_3 (bottom) schemes for $M_\infty = 0.4$ and $\alpha = 5°$*

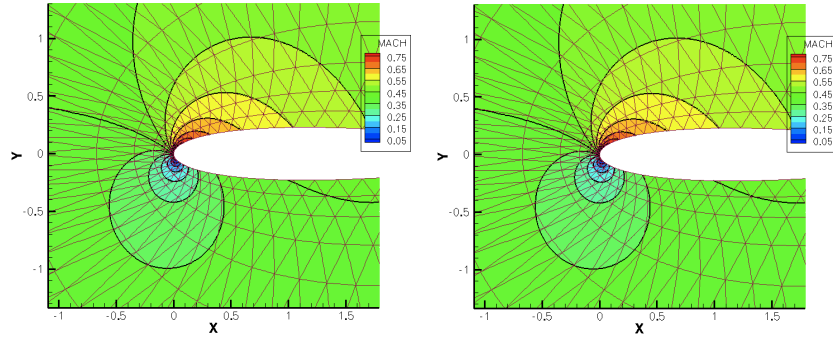American Institute of Aeronautics and Astronautics

Figure 20. *Mach number contours generated using 4th order Discontinuous Galerkin (left) and RT_3 (right) schemes for $M_\infty = 0.4$ and $\alpha = 5°$*

VIII. Conclusions and Future Work

A new variant of the Spectral Difference method which uses Raviart-Thomas elements has been implemented and validated. An existing linear stability analysis study has been extended with an optimal 5 stage 4th order Strong Stability Preserving (SSP) time discretization scheme. The SSP scheme is found to have better performance when compared with 3rd order Shu-RK3 scheme. Stable flux node configurations for the 4th order new SD scheme have been found based on the linear stability analysis. A convergence study has been conducted with the new Spectral Difference scheme for a linear advection problem in the 2-dimensional case. Simulations were done using the 2nd, 3rd and 4th order new Spectral Difference scheme. The results show that full order of convergence is achieved. This motivated us to perform simulations using the new scheme for the more complex case of 2D flow over an airfoil. The Euler equations have been solved around the NACA0012 airfoil for subsonic flow cases. Promising results were obtained using the new Spectral Difference scheme.

Future work should aim at finding a general set of stable flux nodes for 5th and higher order new SD schemes. For solving real life compressible fluid flow problems, the scheme should be equipped with methodologies to deal with discontinuities, like shock waves, in the flow. Furthermore, the scheme needs to be extended to solve the compressible Navier-Stokes equations. These challenges are left for future investigations.

IX. Acknowledgments

References

[1]Liu, Y., Vinokur, M., and Wang, Z. J., "Spectral Difference method for unstructured grids I: Basic formulation," *J. Comp. Phys.*, Vol. 216, No. 2, 2006, pp. 780–801.

[2]May, G. and Jameson, A., "A Spectral Difference Method for the Euler and Navier-Stokes Equations on Unstructured Meshes," AIAA Paper 06-0304, 2006.

[3]Wang, Z. J., Liu, Y., May, G., and Jameson, A., "Spectral Difference Method for Unstructured Grids II: Extension to the Euler Equations," *J. Sci. Comput.*, Vol. 32, No. 1, 2007, pp. 54–71.

[4]May, G., "On the connection between the Spectral Difference method and the Discontinuous Galerkin method," *Commun. Comput. Phys.*, 2010.

[5]Cockburn, B. and Shu, C. W., "The Runge-Kutta Local Projection P^1–Discontinuous–Galerkin Finite Element Method for Conservation Laws," M^2AN, Vol. 25, No. 3, 1991, pp. 337–361.

[6]Cockburn, B. and Shu, C. W., "TVB Runge-Kutta Local Projection Discontinuous Galerkin Finite Element Method for Conservation Laws II: General Framework," *Math. Comp.*, Vol. 52, No. 186, 1988, pp. 411–435.

[7]Cockburn, B. and Shu, C. W., "The Local Discontinuous Galerkin Method for Time-Dependent Convection-Diffusion Systems," *SIAM. J. Numer. Anal.*, Vol. 35, No. 6, 1998, pp. 2440–2463.

[8]Cockburn, B. and Shu, S. W., "The Runge-Kutta Discontinuous Galerkin Method for Conservation Laws V: Multidimensional Systems," *J. Comp. Phys.*, Vol. 141, 1998, pp. 199–224.

[9]Cockburn, B. and Shu, C. W., "Runge-Kutta Discontinuous Galerkin Methods for Convection-Dominated Problems," *J. Sci. Comp.*, Vol. 16, No. 3, 2001, pp. 173–261.

[10]Jameson, A., "A Proof of the Stability of the Spectral Difference Method for All Orders of Accuracy," *J. Sci. Comput.*, DOI 10.1007/s10915-009-9339-4 2009.

[11]den Abeele, K. V., Lacor, C., and Wang, Z. J., "On the Stability and Accuracy of the Spectral Difference Method," *J. Sci. Comput.*, Vol. 37, No. 2, 2008, pp. 162–188.

[12]May, G. and Schöberl, J., "Analysis of a Spectral Difference Scheme with Flux Interpolation on Raviart-Thomas Elements," AICES Technical Report 2010-04/8, Aachen Institute for Advanced Study in Computational Engineering Science, 2010.

[13]Brezzi, F. and Fortin, M., *Mixed and Hybrid Finite Element Methods*, Vol. 15 of *Springer Series in Computational Mathematics*, Springer-Verlag, 1991.

[14]Gottlieb, S. and Shu, C. W., "Total variation diminishing Runge-Kutta schemes," *Math. Comp.*, Vol. 67, 1998, pp. 73–85.

[15]Gottlieb, S., Shu, C. W., and Tadmor, E., "Strong Stability-Preserving High-Order Time Discretization Methods," *SIAM Rev.*, Vol. 43, No. 1, 2001, pp. 89–112.

[16]Spiteri, R. J. and Ruuth, S. J., "A new class of optimal high-order Strong-Stability-Preserving time discretization methods," *SIAM Journal on Numerical Analysis*, Vol. 40, No. 2, 2003, pp. 469–491.

[17]H. Lomax, T. H. Pulliam, D. W. Z., *Fundamentals of Computational Fluid Dynamics*, Springer, 2003.

[18]Karniadakis, G. E. and Sherwin, S., *Spectral/hp Element Methods for Computational Fluid Dynamics*, Oxford University Press, 2nd ed., 2005.

[19]Jameson, A., "Analysis and design of numerical schemes for gas dynamcics 2: Artificial diffusion and discrete shock structure," *Int. J. Comp. Fluid. Dyn.*, Vol. 5, 1995, pp. 1–38.

[20]Balay, S., Buschelman, K., Eijkhout, V., Gropp, W. D., Kaushik, D., Knepley, M. G., McInnes, L. C., Smith, B. F., and Zhang, H., "PETSc Users Manual," Tech. Rep. ANL-95/11 - Revision 2.1.5, Argonne National Laboratory, 2004.

[21]Saad, Y., *Iterative Methods for Sparse Linear Systems*, Society for Industrial and Applied Mathematics, 2nd ed., 2003.

[22]Saad, Y. and Schultz, M. H., "GMRES: A Generalized Minimal Residual Algorithm for Solving Non-Symmetric Linear Systems," *SIAM J. Sci. Stat. Comp.*, Vol. 7, 1986, pp. 856–869.

[23]Dubiner, M., "Spectral Methods on Triangles and Other Domains," *J. Sci. Comput.*, Vol. 6, No. 4, 1991, pp. 345–390.

American Institute of Aeronautics and Astronautics

Appendix

A.   Finding The Transfer Matrix

As given in section II, the solution function is approximated as

$$u_h\left(\xi\right) = \sum_{j=1}^{N_m} u_j l_j\left(\xi\right).$$

(40)

If $\hat{\xi}_j$ are the solution nodes, then the coefficients are given as $u_h\left(\hat{\xi}_j\right) = u_j$. If the flux nodes are denoted as $\breve{\xi}_k$, then the solution variable at flux nodes is given as

$$u_h\left(\breve{\xi}_k\right) = \sum_{j=1}^{N_m} u_j l_j\left(\breve{\xi}_k\right).$$

(41)

Here $l_j\left(\breve{\xi}_k\right)$, the Lagrangian polynomials evaluated at the flux nodes, are unknowns and are found as given below using the Dubiner basis functions, $\chi\left(\xi\right)$, which is a well-known orthogonal basis for triangles.[23] The values of $l_j\left(\breve{\xi}_k\right)$ can be written in the form of a matrix which is called the transfer matrix. The Dubiner basis is obtained from the tensor product of Jacobi polynomials which are defined in the 1D interval [-1,1]. These functions can also be expressed in terms of Lagrangian functions as

$$\chi\left(\xi\right) = \sum_{j=1}^{N_m} \chi_j l_j\left(\xi\right),$$

(42)

where $\chi_j = \chi\left(\hat{\xi}_j\right)$ is evaluated at the solution points. Note that the above equation is an exact relation as both set of functions form a basis in the same polynomial space. The Dubiner basis functions can be evaluated at the flux nodes :

$$\chi\left(\breve{\xi}_k\right) = \sum_{j=1}^{N_m} \chi_j l_j\left(\breve{\xi}_k\right).$$

(43)

Since the Dubiner basis functions at the flux nodes $\chi\left(\breve{\xi}_k\right)$ and those at the solution nodes $\chi\left(\hat{\xi}_j\right)$ are known, the transfer matrix $l_j\left(\breve{\xi}_k\right)$ is obtained by solving the linear system (43) for each distinct flux node $\breve{\xi}_k$. This transfer matrix is used to find the solution at the flux nodes. Since the mesh elements, including the curved ones on the boundary, are mapped to the reference element with the same solution and flux node distribution, the transfer matrix is universal, independent of the cell and so it needs to be stored only once, which is, for the reference element.

B.   Finding The Differentiation Matrix

The vector-valued interpolation basis functions, $\vec{\psi}_k$, and their derivatives can be found by using the fact that any monomial in the Raviart-Thomas (RT) space can be expressed as a linear combination of those basis functions.

$$\vec{\phi}_n\left(\hat{\xi}_j\right) = \sum_{k=1}^{N_m^{RT}} a_{n,k} \vec{\psi}_k\left(\hat{\xi}_j\right),$$

(44)

$$\nabla^\xi \cdot \vec{\phi}_n\left(\hat{\xi}_j\right) = \sum_{k=1}^{N_m^{RT}} a_{n,k} \left(\nabla^\xi \cdot \vec{\psi}_k\right)\left(\hat{\xi}_j\right),$$

(45)

where $a_{n,k} = \vec{\phi}_n\left(\breve{\xi}_k\right) \cdot s_k$ and $\vec{\phi}_n$, $n = 1,2,...,N_m^{RT}$ are the known monomial basis in the RT space. In Eq. (45), since the left hand side and $a_{n,k}$ are known, the divergence of the basis functions $\left(\nabla^\xi \cdot \vec{\psi}_k\right)\left(\hat{\xi}_j\right)$ can be obtained by solving the linear system in the same way as for the transfer matrix.